IEEE Access
Multidisciplinary | Rapid Review | Open Access Journal

Received April 20, 2022, accepted May 21, 2022, date of publication May 30, 2022, date of current version June 3, 2022.

Digital Object Identifier 10.1109/ACCESS.2022.3178737

A Grid Frequency Support Control Strategy of the Three Phase Cascaded H-Bridge Based Photovoltaic Generation System

XUEQING LI[1], JIANYUN CHAI[2], MING LI[3], LIANGRAN LI[1], AND RUI YOU[1]
[1]College of Electrical Engineering, Qingdao University, Qingdao 266071, China
[2]Department of Electrical Engineering, Tsinghua University, Beijing 100084, China
[3]College of Engineering, Ocean University of China, Qingdao 266100, China

Corresponding author: Rui You (yourui1984@163.com)

This work was supported in part by the Shandong Provincial Key Research and Development Program under Grant 2019JZZY010902, in part by the Shandong Provincial Natural Science Foundation under Grant ZR2020ME197, and in part by the National Natural Science Foundation of China under Grant 51761135014.

ABSTRACT Due to advantages such as being clean and safe, photovoltaic (PV) generation has become an effective way to solve the energy crisis and environmental pollution problems. However, the PV inverter does not have inertia and damping characteristics. With the increased penetration of the PV generation into the power system, large-scale PV grid-connection has posed a great challenge to grid frequency stability. The Cascaded H-bridge (CHB) inverter has become a promising candidate for the PV generation system by virtue of advantages such as modular structure and direct grid-connection without power frequency transformers. An inverter control strategy with grid frequency support function is proposed in this paper for the three phase CHB based PV generation system. With the PV string active power reserve, grid frequency dynamic characteristics are improved without energy storage devices. In order to solve the common module power unbalance problem for the CHB topology, the PV string output power is controlled to be balanced with the reserved power distribution control between PV strings proposed in this paper. The H-bridge inverter input power balance is maximized, and balanced three phase grid-connected current output is achieved. The over-modulation risk of H-bridge modules is reduced. At last, simulation models are built in Matlab/Simulink, and a 10kW experimental platform is also built. The effectiveness of the control strategy proposed is validated by simulation and experimental results.

INDEX TERMS Active power reserve, cascaded H-bridge inverter, frequency support, photovoltaic power generation.

I. INTRODUCTION

In order to solve global energy crisis and environmental problems, renewable energy sources, especially photovoltaic (PV) generation has been developed rapidly during last decades [1], [2]. With the increased PV generation penetration into the power system, the proportion of conventional synchronous generators has been reduced dramatically. This leads to the weakened power system response to power fluctuations and system faults, bringing potential risks to the grid stability [3].

Different from wind turbines, there are no mechanical rotation devices in the PV generation system. Therefore, no kinetic energies, such as ones stored in the turbine and drive train of wind turbines, can be released to support grid frequency for the PV generation system [4]. In addition, PV cells usually operate at maximum power point tracking (MPPT) mode [5]. When the grid frequency drops, their output active power can't be increased to execute the frequency response control.

To address the abovementioned issue, grid frequency support from the PV generation system has attached wide attention [6]–[9]. The fast output power change of the PV generation system can reduce the power unbalance in the grid, contributing to the improvement of grid frequency dynamic characteristics. Inertia and damping characteristics were emulated with the virtual synchronous generator (VSG) control of the battery energy stored quasi-Z source inverter

The associate editor coordinating the review of this manuscript and approving it for publication was B. Chitti Babu.

based PV generation system in [10]. A decentralized VSG-based adaptive coordinated control strategy was proposed for islanding microgrids consisting of PV generation combined with battery energy storages in [11]. Dynamic performances of the system were enhanced. Nevertheless, the inverter output power change was from energy storage devices in the schemes above, resulting in the increased system volume, weight, cost and maintenance workload. The PV cell operation point can be moved from the maximum power point, meaning that it operates at deload mode, and some power is reserved. In terms of control strategies, a predictive PV inverter control method, coupled with a maximum power point estimation method was proposed in [12]. Fast and accurate active power response to a demanding range of grid frequency events was provided. A novel adaptive PV frequency control strategy was proposed to reserve the minimum power for grid frequency support in [13]. Based on a machine learning model trained, system frequency response under various system conditions was predicted, and an adaptive allocation of PV headroom reserves was made. An event-triggering power reserve control for the three phase two-stage PV generation system, consisting of two operation modes, was proposed in [14] to track the maximum power point accurately with fast dynamics or increase output power with reservation. The PV generation system was regulated as an adaptable current source with reserved power for grid frequency support.

In order to connect the medium voltage grid directly, a cascaded H-bridge (CHB) multilevel inverter can be used as the grid-connection interface in the PV generation system. PV strings fulfill the requirement of independent DC sources supplying for the CHB topology [15]. The voltage stress of switching devices is reduced, and the inverter output voltage and current quality is improved [16]. With the direct connection between PV strings and DC-links, DC-DC converters can be eliminated, leading to further reduced system loss and volume, and enhanced efficiency [17]. Few literatures have studied the grid frequency support control of the CHB based PV generation system. An H-bridge inverter, directly connected to a battery is added in a single phase CHB based PV generation system in [18]. Each PV string operates at its maximum power point, and the battery can be easily adopted to snubber the power difference between power demands and system generation. However, increased system output power when supporting grid frequency is still from energy storage devices. A power reserve control strategy was proposed for the single phase CHB converter in [19]. The PV cell with the maximum output power is selected as the reserved cell. When the grid frequency drops, the reserved power is fast released to support grid frequency. Nevertheless, over-modulation risks of H-bridge modules corresponding to other cells are increased. Furthermore, the single phase PV generation system was chosen in both literatures above. In the more common three phase system, the power unbalance between H-bridge modules introduces unbalanced three phase transmission power and grid-connected current. Although the three phase grid-connected current unbalance can be improved with the zero-sequence voltage injection, the balanced three phase grid-connected current can't always be obtained due to the DC-link voltage limit, when the three phase transmission power being unbalanced severely [20]–[22]. Normally, a three phase CHB based PV generation system should be controlled to maximize the solar energy captured. The three phase transmission power is expected to achieve maximum balance during both power reserve and grid frequency support operation. High quality grid-connected current should always be maintained during the operation stages above. This is the main challenge for the CHB based PV generation system at deload mode, compared with common PV generation systems.

Based on the analysis above, a grid frequency support control strategy of the three phase CHB based PV generation system is proposed in this paper. During power reserve operation, the reserved power required is obtained with the coordinated control of all PV strings. The system output power is increased fast according to the grid frequency change when participating in grid frequency support, leading to the improvement of grid frequency dynamic characteristics. Different from common methods that controlling three phase grid-connected current to be balanced after the occurrence of unbalanced three phase transmission power, the main contribution of this paper is proposing a control method to regulate the transmission power between modules to achieve maximum balance. The reserved power is distributed between modules only with the correction of DC-link voltage references. The maximum balance of the transmission power between modules and three phase grid-connected current can be ensured, resulting in the reduced H-bridge inverter over-modulation risk and improved grid-connected current quality. Finally, the effectiveness of the control strategy proposed is validated with both simulation and experimental results.

II. SYSTEM TOPOLOGY AND ANALYSIS ON DELOAD MODE OPERATION

A. TOPOLOGY OF THE CHB BASED PV GENERATION SYSTEM

The topology of the three phase CHB based PV generation system with Star-connection is shown in Fig. 1. An H-bridge inverter is connected to a PV string directly to form an H-bridge module. n H-bridge modules are cascaded in each phase. C and L are the DC-link filter capacitance and grid side filter inductance, respectively. I_{PVxj} and V_{dcxj} are the output current and DC-link voltage of the PV string in the jth H-bridge module in Phase x ($x = A, B, C, j = 1, 2, \ldots, n$). v_{x} and i_{x} are the three phase grid voltage and grid-connected current, respectively. With the three level voltage obtained from each H-bridge module, $2n + 1$ level system output voltage expressed below can be achieved.

$$V_{xN} = \sum_{j=1}^{n} m_{xj} V_{dcxj} \tag{1}$$

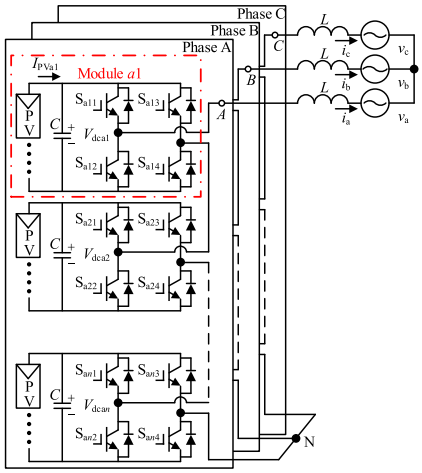

FIGURE 1. Three phase CHB based PV generation system topology.

where m_{xj} is the modulation index of each H-bridge module. According to the Kirchhoff law, the relationship between system output voltage and current is:

$$L\frac{d}{dt}\begin{bmatrix} i_a \\ i_b \\ i_c \end{bmatrix} = \begin{bmatrix} \sum m_{aj}V_{dcaj} \\ \sum m_{bj}V_{dcbj} \\ \sum m_{cj}V_{dccj} \end{bmatrix} - \begin{bmatrix} v_a \\ v_b \\ v_c \end{bmatrix} \tag{2}$$

$$C * dV_{dcxj}/dt = I_{PVxj} - m_{xj}i_x \tag{3}$$

When the output power decreases in some phase due to partial shading, accumulated dust, and so on, unbalanced three phase transmission power can introduce unbalanced three phase grid-connected current. Zero sequence voltage injection methods such as fundamental frequency zero-sequence injection, weighted min-max zero-sequence injection, double 1/6 three harmonic injection, optimal zero-sequence injection can be applied to achieve balanced three phase grid-connected current output in the case of unbalanced three phase transmission power [23]. However, due to DC-link voltage limit, only the power unbalance below 20% can be handled even with the optimal zero-sequence voltage injection method with the best balancing capability [24]. Therefore, to address the three phase grid-connected current unbalance issue, it is essential to control all PV string output power to achieve maximum balance.

B. ANALYSIS ON STABLE DELOAD OPERATION AREA

One *P-V* characteristic curve of a PV string is shown in Fig. 2. The PV string output power ranges from 0 to P_{mpp}, the maximum output power corresponding to the maximum power point. Therefore, the power reserve can be achieved by changing its operation point from the maximum power point. During grid frequency support, the reserved power is released with the increased PV string output power by changing its operation point. There are two voltages corresponding to every power point except the maximum one. On the left of the maximum power point, the relationship between the

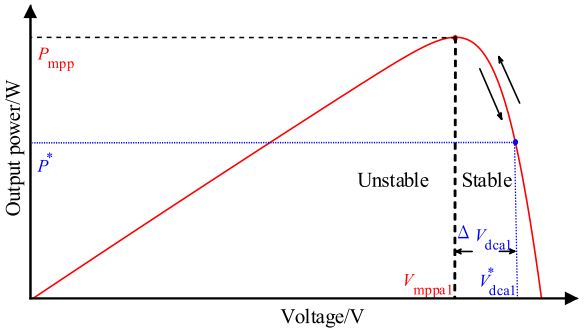

FIGURE 2. A P-V operation curve of a PV string.

PV string voltage V_{dc} and its output power P_{pv} is expressed as $dP_{PV}/dV_{dc} > 0$. On the right side, it is expressed as $dP_{PV}/dV_{dc} < 0$. The PV string operation area should be selected at deload mode for its stable operation.

The PV string output power is expressed in equation (4) according to the power flow relationship on both sides of the DC-link capacitor.

$$\begin{cases} P_{PV} = P_{out} + P_C \\ P_C = V_{dc}C * dV_{dc}/dt \end{cases} \tag{4}$$

P_{out} is the H-bridge module output power. $P_c$is the capacitor charging or discharging power. After the linearization of any operation point (V_0, P_0) on the operation curve, equation (5) can be obtained.

$$V_0C\frac{d\Delta V_{dc}}{dt} - \frac{dP_{PV}}{dV_{dc}}\Delta V_{dc} = 0 \tag{5}$$

The eigenvalue is:

$$\lambda = \frac{1}{V_0C}\frac{dP_{PV}}{dV_{dc}} \tag{6}$$

The system can operate stably only when all eigenvalues of its characteristic equation are negative real numbers or conjugate complex numbers with negative real parts. Therefore, the PV string should be controlled to operate on the right of the maximum power point at deload mode.

III. OVERALL CONTROL OF THE THREE PHASE CHB BASED PV GENERATION SYSTEM

The overall control diagram of the three phase CHB based PV generation system is shown in Fig. 3. The grid-connected current is controlled with the voltage-current double closed-loop control. The sum of all DC-link voltages is stabilized with outer voltage loop. Firstly, a moving average filter (MAF) is used to eliminate DC-link voltage ripple with double grid frequency. All $3n$ DC-link voltages V_{dcfxi} and their references V^*_{dcfxi} are summed respectively to calculate the corresponding average values, V_{dc-avg} and V^*_{dc-ref}. With the voltage error, the grid-connected current d-axis component reference i^*_d is determined from a PI controller. The q-axis component reference i^*_q is calculated according to the system output reactive power command

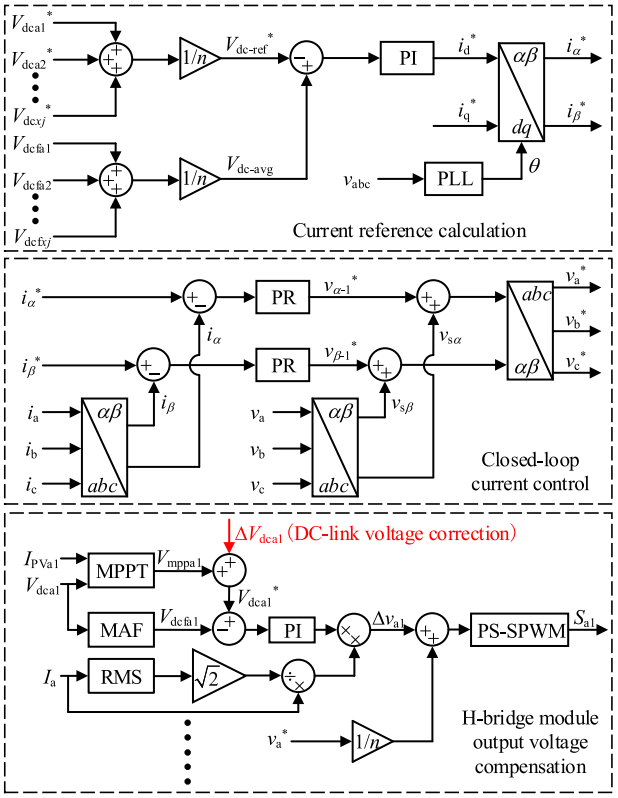

FIGURE 3. Overall control diagram of the CHB based PV generation system.

from the grid. Since the AC signal zero steady error can be obtained with a proportional resonant (PR) regulator, it is chosen to achieve the closed-loop current control in the $\alpha\beta$ coordination system. Therefore, complex coordination transformation and decoupled control can be avoided, leading to improved system dynamic characteristics. The angle used in the coordination transformation is obtained based on the grid voltage measured with a phase locked loop (PLL). A feedforward voltage compensator is implemented by adding the filter inductance voltage reference from the PR regulator to the grid voltage components in the $\alpha\beta$ coordination system to avoid high transient current during grid voltage sags [17].

Each H-bridge inverter voltage reference is calculated by dividing v_x^* by n, which is the number of cascaded modules in one phase. In order to maintain stable system operation with different transmission power between modules, H-bridge inverter voltage references should be modified. Since the sum of all $3n$ DC-link voltages has been controlled to track its reference in the outer voltage loop, $3n$-1 voltages are selected at random and controlled to track their corresponding references, resulting in the closed-loop control of all DC-link voltages. Take the first H-bridge inverter in Phase A as an example, a PI regulator is used to calculate the amplitude of its compensation voltage with the error between V_{dca1}^* and V_{dcfa1}. The compensation voltage Δv_{a1} is obtained by multiplying the unit sine signal with the same phase as the output current in Phase A. The H-bridge inverter final output voltage reference is calculated by adding Δv_{a1} to v_{a}^*/n. Similarly, all other selected H-bridge inverter output voltage references are obtained. The compensation control is not executed for the unselected H-bridge module, in other words, its compensation voltage is set 0. At last, phase-shifted sinusoidal pulse width modulation (PS-SPWM) is used to generate gate signals of all $3n$ H-bridge inverters.

Power reserve and grid frequency support can be achieved only by modifying each DC-link voltage reference, meaning that adding ΔV_{dca1} to the original voltage reference in Fig. 3. Therefore, the consistency of the control strategy can be ensured. The selection of modified H-bridge modules and the modification value calculation will be illustrated in detail below.

IV. CALCULATION OF DC-LINK VOLTAGE REFERENCE MODIFICATION DURING POWER RESERVE AND GRID FREQUENCY SUPPORT

A. RESERVED POWER CALCULATION

During power reserve operation, three phase CHB based PV generation system reserved power $P'_{\mathrm{res}}(t)$ can be calculated according to [25]. During grid frequency support operation, the increased output power reference $\Delta P_{\mathrm{s}}(t)$ is shown below based on the grid frequency measured.

$$\Delta P_s(t) = -J\omega_0 \frac{d\omega_g(t)}{dt} - k\omega_0(\omega_g(t) - \omega_0) \tag{7}$$

k and J are the active power droop coefficient and moment of inertia, respectively. $\omega_{\mathrm{g}}(t)$ and ω_0 are the grid frequency and its rated value, respectively. During grid frequency support operation, the system reserved power reference is calculated in equation (8) according to $\Delta P_{\mathrm{s}}(t)$ obtained above and $P'_{\mathrm{res}}(t_0)$, which is its initial value at the beginning moment of grid frequency support t_0.

$$P_{res}(t) = \begin{cases} P'_{res}(t)\,, & \textit{Power reserve} \\ P'_{res}(t_0) - \Delta P_s(t)\,, & \textit{Grid frequency support} \end{cases} \tag{8}$$

B. SELECTION OF POWER RESERVE UNITS AND DISTRIBUTION OF RESERVED POWER

In order to achieve the transmission power balance between H-bridge modules during power reserve and grid frequency support, a power distribution control method is proposed to track the reserved power reference $P_{\mathrm{res}}(t)$. MPPT control is executed at some interval, such as 10 min, to obtain the maximum available output power of all PV strings. Based on the power obtained, PV strings at deload mode are selected, and the output power reference P^* is calculated according to the flow chart shown in Fig. 4.

Firstly, each PV string maximum available output power is sorted in descending order to form an array $P[1 \ldots 3n]$. The difference between adjacent sorted power is calculated, and the result $P[i]$-$P[i+1]$ is saved to an array $\Delta P[1 \ldots 3n\text{-}1]$, which is the available reserved power if

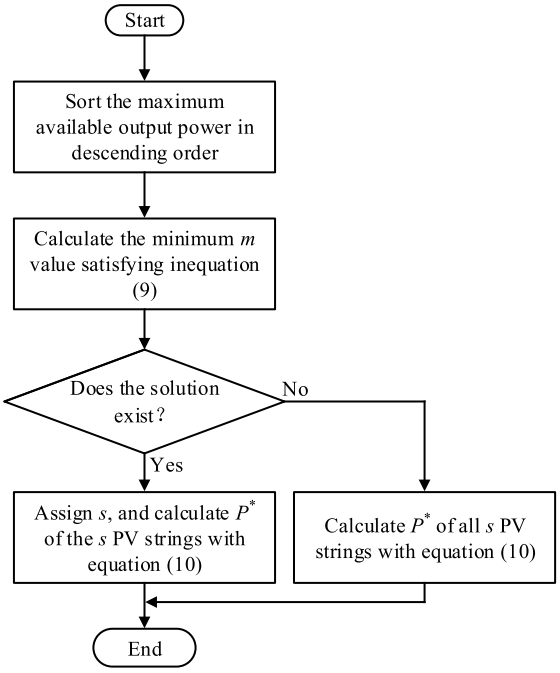

FIGURE 4. Flow chart of output power reference calculation.

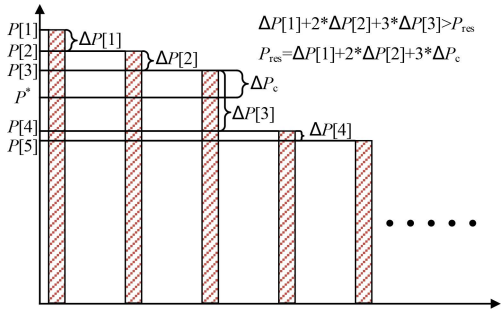

FIGURE 5. Distribution of the reserved power.

reducing the corresponding PV string output power from $P[i]$ to $P[i+1]$. According to the reserved power reference $P_{\text{res}}(t)$ in equation (8), the minimum m value satisfying inequality (9) is calculated, and the result is saved to a variable s. The corresponding PV strings are selected as the power reserve units.

$$\sum_{i=1}^{m} i * \Delta P[i] \geq P_{res}(t) \tag{9}$$

m is an integer between 1 and $3n$-1, and s is the number of modules at deload mode. If inequality (9) can't be satisfied even when $m = 3n$-1, all PV strings should operate at deload mode. For example, it is assumed that all PV string maximum available output power is shown in Fig. 5. Inequality (9) is satisfied when $m = 3$, and the three PV strings, whose maximum available output power corresponding to $P[1]$, $P[2]$ and $P[3]$, are controlled to operate at deload mode. The other PV strings still operate at MPPT mode.

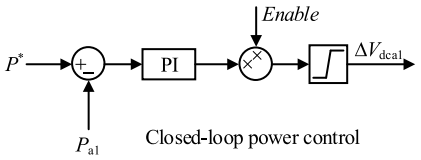

FIGURE 6. DC-link voltage compensation control.

Then, output power references of the selected modules at deload mode are calculated. When some PV strings operate at deload mode, their output power references are same. When all PV strings operate at deload mode, all output power references are same. The output power reference P^* of the modules at deload mode is:

$$P^* = \begin{cases} \left(\sum_{i=1}^{s} i * \Delta P[i] - P_{res}(t)\right) \Big/ s + P[s+1], \\ \qquad\qquad\qquad\qquad \textit{minimal } m \textit{ exists} \\ \left(\sum_{i=1}^{3n} P[i] - P_{res}(t)\right) \Big/ 3n, \quad \textit{no solution} \end{cases} \tag{10}$$

C. MODIFICATION OF DC-LINK VOLTAGE REFERENCES

According to the calculated output power reference P^*, the closed-loop power control is executed for the modules selected. PI regulators are used to calculate DC-link voltage modification values. For example, if the PV string corresponding to the first H-bridge module in Phase A operates at deload mode in Fig. 6, its closed-loop power control is enabled. The DC-link voltage modification value ΔV_{dca1} is calculated with a PI regulator, whose input is the error between the actual output power P_{a1} and its reference P^*. Then, ΔV_{dca1} is added to V_{mppa1}, corresponding to the module maximum power point voltage, to obtain the final DC-link voltage reference. At last, the PV string operates on the right of the maximum power point in Fig. 2, and the output power is P^*.

It should be noted that the three phase CHB based PV generation system with the proposed control strategy still can contribute to the improvement of grid frequency dynamic characteristics when the grid frequency increases. Furthermore, the maximum balance of the transmission power between modules and three phase grid-connected current can still be maintained.

V. SIMULATION ANALYSIS

A three phase CHB based PV generation system simulation model is built in Matlab/Simulink to verify the effectiveness of the control strategy proposed. The 1Soltech 1STH-215-P PV cell model in the Simulink library is used. Each PV string is composed of 32 × 8 cells, and the rated power is 55 kW with the temperature 25 ° and illumination 1000 W/m^2. The grid is modeled with a synchronous generator including an excitation regulator and a speed governor. The

TABLE 1. Main simulation parameters.

Parameters	Values
Grid line voltage RMS value/V	690
Grid rated frequency/Hz	50
Number of H-bridge modules in each phase	3
Grid side filter inductance/mH	1.3
DC-link capacitor/mF	4.7
Droop coefficient	99.55
Moment of inertia/kg·m^2	24

system main parameters are shown in Tab. 1. The ambient temperature is kept constant, 25 °. Firstly, all PV strings operate at MPPT mode. The power reserve control is executed at 1 s. The reserved power is set 10% of the system output power. At 2 s, a 150 kW load is connected to the grid. The three phase CHB based PV generation system is controlled to support grid frequency with the control strategy proposed. Different illuminations are set for some PV strings to emulate their deload operation, and all PV strings deload operation, respectively.

A. SOME PV STRINGS OPERATING AT DELOAD MODE

The illumination corresponding to the jth H-bridge module in Phase x is expressed as S_{xj}. The illumination is set below: $S_{a1} = 700$ W/m^2, $S_{a2} = 900$ W/m^2, $S_{a3} = 970$ W/m^2, $S_{b1} = 800$ W/m^2, $S_{b2} = 950$ W/m^2, $S_{b3} = 1000$ W/m^2, $S_{c1} = 750$ W/m^2, $S_{c2} = 850$ W/m^2, $S_{c3} = 1000$ W/m^2. Simulation results are shown in Fig. 7, in which each DC-link voltage shown in (a), PV string output power shown in (b), the sum of all PV strings output power shown in (c), grid frequency shown in (d), and grid-connected current shown in (e). It can be observed that each PV string operates at its maximum power point individually with the MPPT control before 1 s, leading to the maximum system output power. All PV strings except the ones corresponding to Module $a1$, $b1$, and $c1$ whose operation modes remain unchanged, are selected as power reserve units. Power reserve with 10% system output power is achieved by increasing their terminal voltages. More power losses occur for the modules with more output power when operating at MPPT mode. The transmission power unbalance between H-bridge modules is reduced. The power loss in each PV string depends on its maximum available output power difference and system reserved power demand. The connection of the load leads to the dropping of the grid frequency from 2 s. Based on the power calculation in equation (8), the reserved power has been distributed between H-bridge modules with the control strategy proposed during grid frequency support. At last, the PV string corresponding to Module $c2$ operates at MPPT mode again, and the output power of the rest five PV strings at deload mode is increased to the same value. The whole system output power is increased fast from 390 kW to

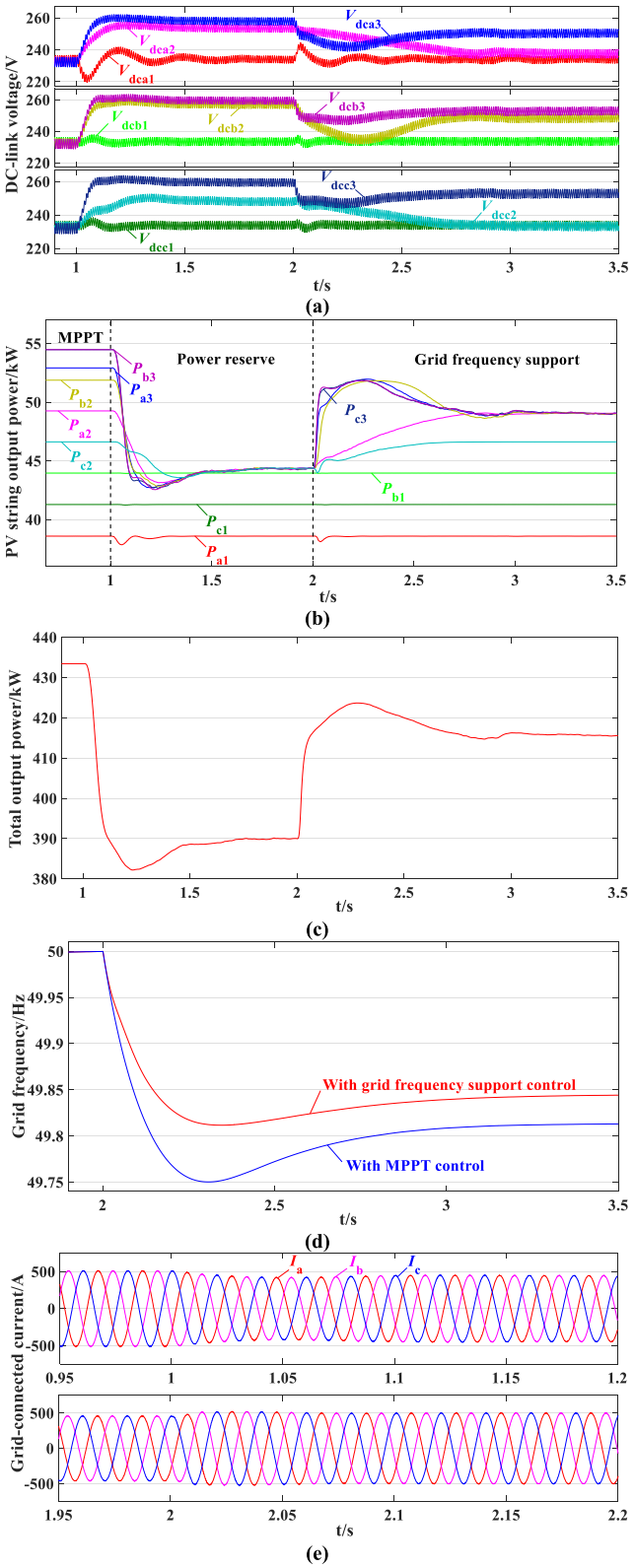

FIGURE 7. Condition when some PV strings operating at deload mode. (a) DC-link voltage corresponding to each H-bridge module. (b) PV string output power. (c) Sum of all PV strings output power. (d) Grid frequency. (e) Grid-connected current.

416 kW. The rate of change of frequency is reduced, and the nadir is increased from 49.75 Hz to 49.81 Hz. The grid inertia

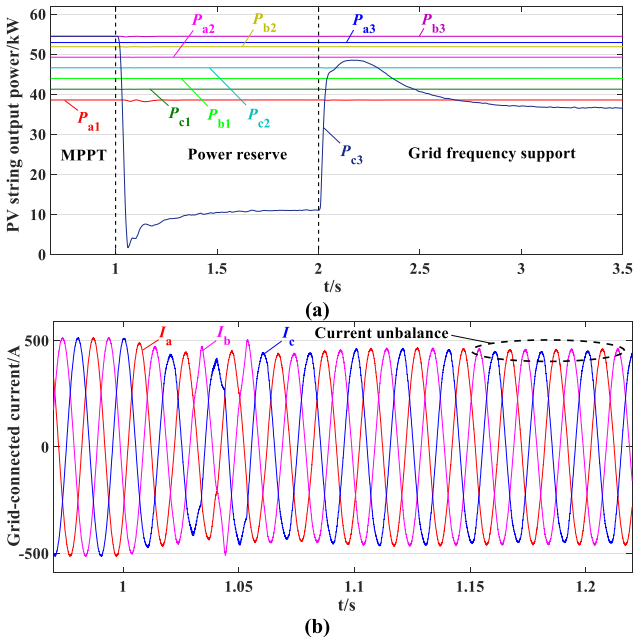

FIGURE 8. Simulation results with the control strategy in [19]. (a) PV string output power. (b) Grid-connected current.

and damping are enhanced, and the obvious improvement of grid frequency dynamic characteristics is achieved. When the control method in [19] is used in the same condition, each PV string output power and grid-connected current are shown in Fig. 8. Since only Module $c3$ with maximum output power at MPPT mode is selected as the power reserve unit, its dramatically reduced output power exacerbates the power unbalance between H-bridge modules during power reserve operation. This results in the occurrence of the over-modulation in the modules with more output power, and the distortion and unbalance of three phase grid-connected current are caused. By contrast, the power balance between modules is maintained, and the over-modulation and current distortion are avoided with the control strategy proposed in this paper. The system three phase grid-connected current has always been kept balanced.

B. ALL PV STRINGS OPERATING AT DELOAD MODE

The illumination is set 1000 W/m^2 for all PV strings except the three ones whose settings are below: $S_{a1} = 900$ W/m^2, $S_{b2} = 950$ W/m^2, $S_{c2} = 900$ W/m^2. Simulation results are shown in Fig. 9. Due to the reduced difference between PV string maximum available output power, even though all PV strings are controlled to reduce output power to the value corresponding to the maximum available output power of Module a1 and c2 (minimum value among all modules at MPPT mode), 10% power reserve can still not be satisfied. Therefore, all PV strings are controlled to operate at deload mode. The reserved power requirement is fulfilled, and the transmission power between modules is balanced totally. At last, all PV strings are controlled to increase the output power fast to response to the grid frequency

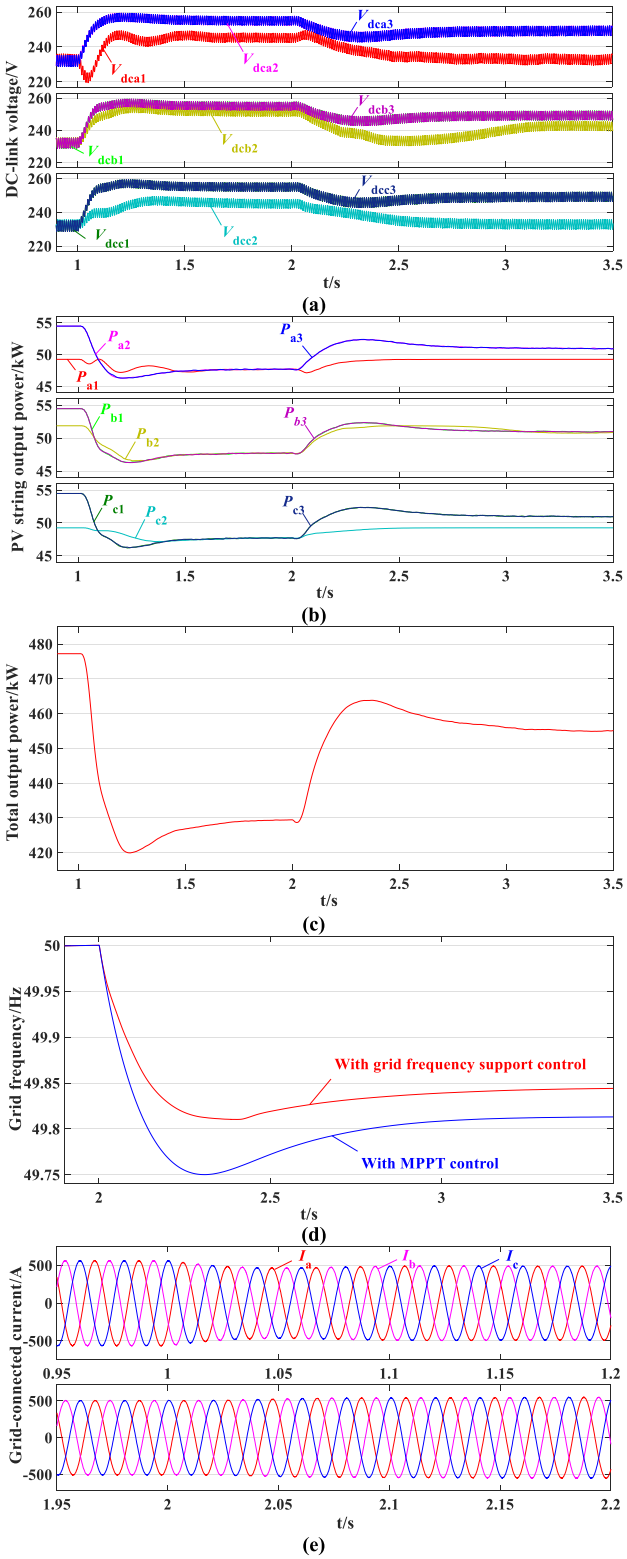

FIGURE 9. Condition when all PV strings operating at deload mode. (a) DC-link voltage corresponding to each H-bridge module. (b) PV string output power. (c) Sum of all PV strings output power. (d) Grid frequency. (e) Grid-connected current.

dropping. The minimum grid frequency is increased from 49.75 Hz to 49.81 Hz, and the balanced transmission power and grid-connected current have been maintained.

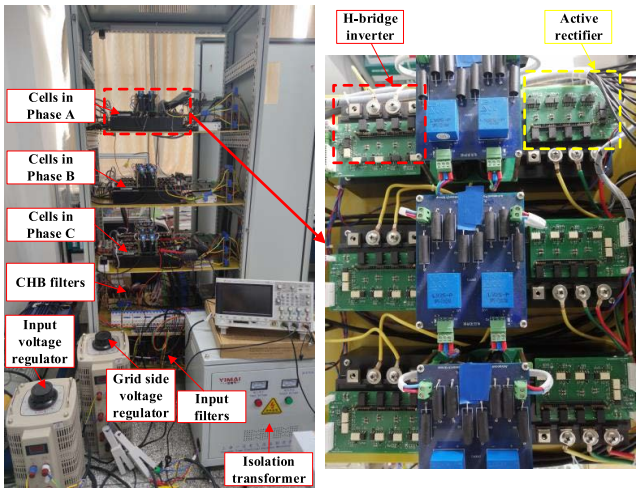

FIGURE 10. Experimental platform of the three phase CHB based PV generation system built.

VI. EXPERIMENTAL VALIDATION

A 10 kW three phase CHB based PV generation system experimental platform shown in Fig. 10 is also built to validate the control strategy proposed. There are three modules in each phase. Each module includes two back-to-back IGBT power cells (PM25RL1A120). One power cell is controlled as an active rectifier to emulate power output characteristics of the PV string. Two bridges arms in the other one are used to form an H-bridge inverter. Three H-bridge inverters in one phase are cascaded as a CHB inverter. The nine active rectifiers are fed by the nine secondary side windings of an isolation transformer. The transformer is connected to an input voltage regulator. The cascaded H-bridge inverter is coupled with grid by the other voltage regulator, which also provides the galvanic isolation. Four DSP (TMS320F28335) + FPGA (XC3S400-PQG208EGQ) control boards are used to implement the control algorithm and generate the PWM signals. Three active rectifiers in one phase and all H-bridge inverters are controlled by one control board, respectively [16]. The main parameters are shown in Tab. 2.

At First, all PV strings are emulated to operate at MPPT mode. All DC-link voltages are controlled to be 50 V. The RMS value of the rectifier input three phase current of the first module in Phase C is set 3.07 A to emulate the output power of the PV string corresponding to Module $c1$ being 130 W. The corresponding RMS values of the other eight modules are all set 2.36 A to emulate the output power being 100 W. Then, the system deload operation is emulated. The reserved power is set 10% of the output power, 93 W. Each module input current is used to reflect its transmission power in this paper.

With the reserved power distribution method proposed in this paper, the input current of Module $b1$ and $c1$, grid-connected current in Phase B and C and DC-link voltage corresponding to Module $b1$ and $c1$ are shown in Fig. 11. RMS values of all nine rectifiers input three phase current

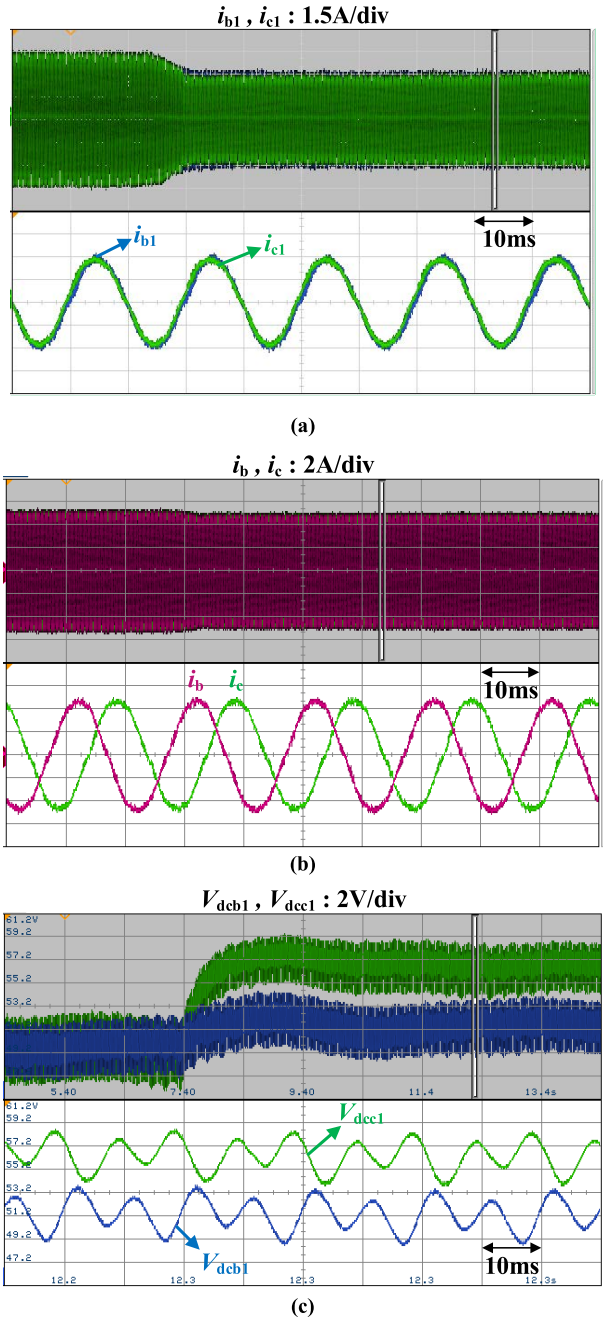

FIGURE 11. Transition from MPPT mode to deload mode. (a) Module b1 and c1 input current. (b) Grid-connected current in Phase B and C. (c) DC-link voltage corresponding to Module b1 and c1.

are all 2.19 A during power reserve operation. The reserved power requirement is fulfilled successfully. Furthermore, the transmission power balance between modules and balanced three phase grid-connected current output are achieved. The oscillation with 100 Hz of double grid frequency is observed. The average voltage is increased from 50 V to about 57.1 V and 51.8 V, respectively to emulate the PV strings deload operation, and the stable DC-link voltage is kept successfully.

When the control method in [19] is used in the same condition, the input current of Module $b1$ and $c1$ and

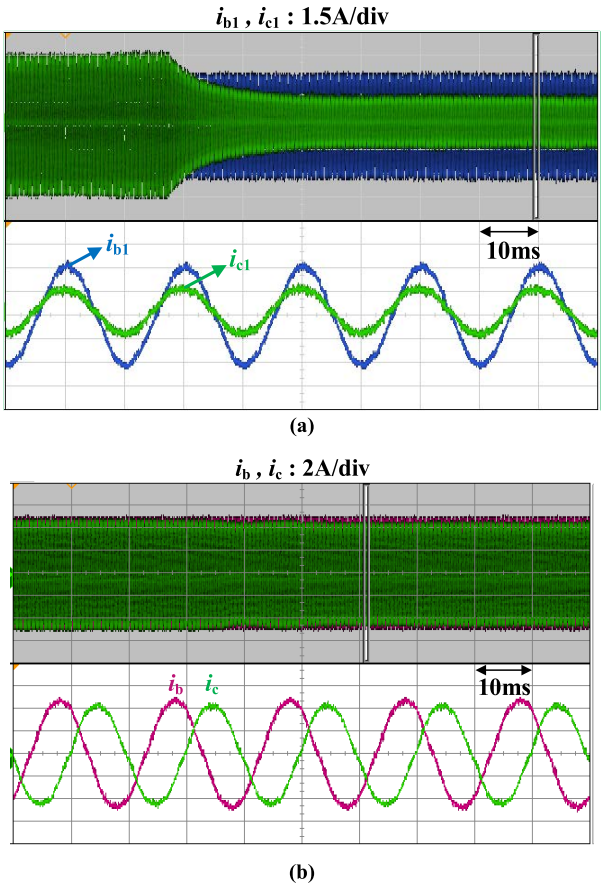

FIGURE 12. Experimental results with the control strategy in [19]. (a) Module b1 and c1 input current. (b) Grid-connected current in Phase B and C.

grid-connected current in Phase B and C are shown in Fig. 12. The reserved power is achieved only with the deload operation of Module $c1$, with maximum transmission power during MPPT operation. Therefore, its transmission power is reduced to 37 W, and the RMS value of the corresponding rectifier input three phase current is reduced to 0.9 A. The output power of the other eight modules is kept constant. Although the reserved power requirement is fulfilled, the transmission power difference between Module $c1$ and the other modules is large, leading to the unbalanced three phase grid-connected current. The effectiveness and advantage of the control strategy proposed have been validated.

At last, the system output power is controlled to increase 60 W fast to emulate the grid frequency support control. The input current of Module $b1$ and $c1$, the grid-connected current in Phase B and C and DC-link voltage corresponding to Module $b1$ and $c1$ are shown in Fig. 13. It can be observed that the rapid increase of the system output power is achieved with the decrease in DC-link voltages. At the same time, the transmission power and three phase grid-connected current are kept balanced with the control strategy proposed.

Overall, from the simulation results and experimental results above, the effectiveness of the proposed grid

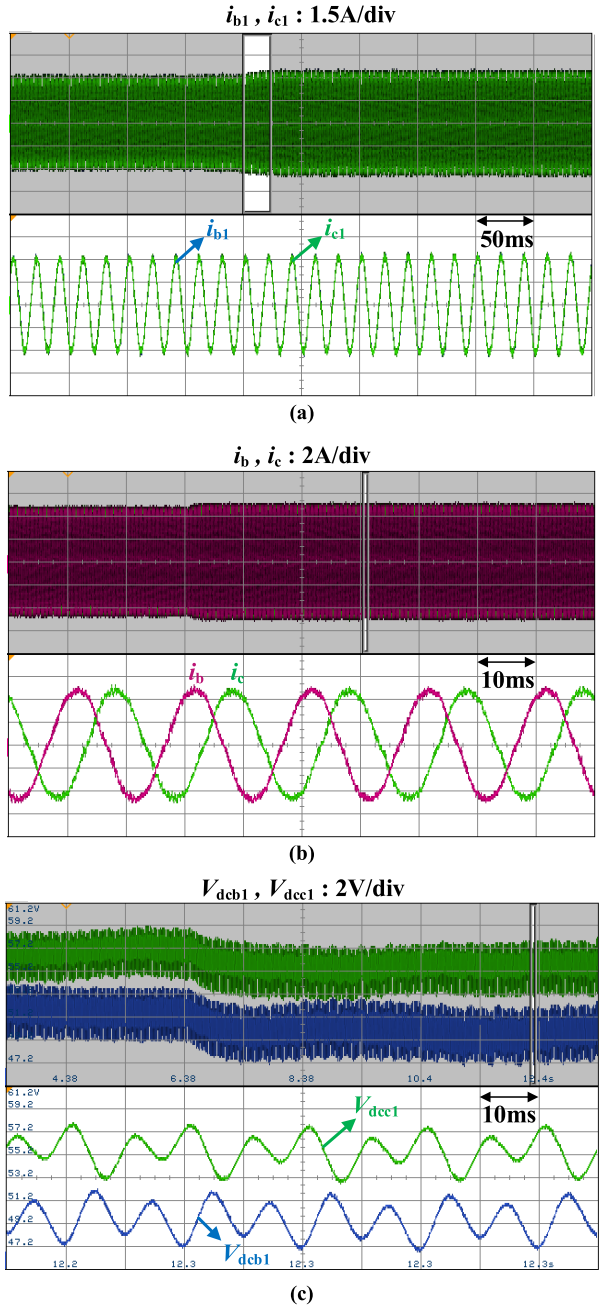

FIGURE 13. Transition from deload mode to grid frequency support mode. (a) Module b1 and c1 input current. (b) Grid-connected current in Phase B and C. (c) DC-link voltage corresponding to Module b1 and c1.

frequency support control strategy of the three phase CHB based PV generation system has been validated. During power reserve operation, the reserved power requirement is fulfilled. Furthermore, the maximum balance of PV strings output power between modules with the coordinated control of their operation points is achieved. Once the grid frequency dropping is detected, the grid frequency dynamic characteristic improvement is achieved with the release of the reserved power. The transmission power balance can still be maintained, leading to maximum and balanced three phase grid-connected current output.

If partial shading occurs, the power balance control between modules during both power reserve and grid frequency support can still be achieved after updating each PV string maximum available output power next cycle. This means that the control strategy proposed is still valid. Before the power updating, the control performance of the power balance will be affected due to the error between the PV string maximum available output power used and its actual value. However, it can be improved by reducing time interval of the MPPT control to accelerate the power updating.

VII. CONCLUSION

A grid frequency support control strategy of the three phase CHB based PV generation system is proposed in this paper to maintain its stable operation at MPPT, deload and grid frequency support modes. During MPPT operation, each PV string maximum power output and the system maximum power output are achieved by regulating each DC-link voltage reference. The reserved power requirement is fulfilled by changing the PV string operation point. When the grid frequency drops, the reserved power is released to improve grid frequency dynamic characteristics. To address the power unbalance issue between H-bridge modules, the coordinated control of all PV strings is achieved only by modifying DC-link voltage references. Maximum transmission power balance between H-bridge modules and balanced three phase grid-connected current are obtained. The H-bridge module over-modulation risk is reduced, and the consistency of the control strategy has been ensured. The simulation and experimental results validate that the grid frequency has been supported effectively, and the three phase grid-connected current has always been balanced with the control strategy proposed.

The PV string output power only depends on the temperature and illumination in the model built. The model modification to emulate the partial shading condition accurately, tests with actual PV cells on the experimental platform, and the deep analysis of the control parameter's influence on the system stability will be the topics of future papers.

REFERENCES

[1] H. Daneshi, "Overview of renewable energy portfolio in CAISO—Operational and market challenges," in *Proc. IEEE Power Energy Soc. Gen. Meeting (PESGM)*, Portland, OR, USA, Aug. 2018, pp. 1–5.

[2] E. Kabir, P. Kumar, S. Kumar, A. A. Adelodun, and K.-H. Kim, "Solar energy: Potential and future prospects," *Renew. Sustain. Energy Rev.*, vol. 82, pp. 894–900, Feb. 2018.

[3] Q.-C. Zhong, "Power-electronics-enabled autonomous power systems: Architecture and technical routes," *IEEE Trans. Ind. Electron.*, vol. 64, no. 7, pp. 5907–5918, Jul. 2017.

[4] R. You, B. Barahona, J. Chai, N. A. Cutululis, and X. Wu, "Improvement of grid frequency dynamic characteristic with novel wind turbine based on electromagnetic coupler," *Renew. Energy*, vol. 113, pp. 813–821, Dec. 2017.

[5] J. Jiang, T. Zhang, and D. Chen, "Analysis, design, and implementation of a differential power processing DMPPT with multiple buck–boost choppers for photovoltaic module," *IEEE Trans. Power Electron.*, vol. 36, no. 9, pp. 10214–10223, Sep. 2021.

[6] J. Zhang, L. Qu, R. Pestana, F. Luan, and L. Yang, "Dynamic frequency support by photovoltaic generation with 'synthetic' inertia and frequency droop control," in *Proc. IEEE Conf. Energy Internet Energy Syst. Integr. (EI)*, Beijing, China, Nov. 2017, pp. 1–6.

[7] Q. Peng, Y. Yang, T. Liu, and F. Blaabjerg, "Coordination of virtual inertia control and frequency damping in PV systems for optimal frequency support," *CPSS Trans. Power Electron. Appl.*, vol. 5, no. 4, pp. 305–316, Dec. 2020.

[8] Q. Li and M. E. Baran, "A novel frequency support control method for PV plants using tracking LQR," *IEEE Trans. Sustain. Energy*, vol. 11, no. 4, pp. 2263–2273, Oct. 2020.

[9] B.-I. Craciun, T. Kerekes, D. Sera, and R. Teodorescu, "Frequency support functions in large PV power plants with active power reserves," *IEEE J. Emerg. Sel. Topics Power Electron.*, vol. 2, no. 4, pp. 849–858, Dec. 2014.

[10] W. Liang, Y. Liu, and Y. Shen, "Active power control integrated with reactive power compensation of battery energy stored quasi-Z source inverter PV power system operating in VSG mode," *IEEE J. Emerg. Sel. Topics Power Electron.*, early access, Dec. 22, 2021, doi: 10.1109/JESTPE.2021.3137397.

[11] M. Mao, C. Qian, and Y. Ding, "Decentralized coordination power control for islanding microgrid based on PV/BES-VSG," *CPSS Trans. Power Electron. Appl.*, vol. 3, no. 1, pp. 14–24, Mar. 2018.

[12] A. F. Hoke, M. Shirazi, S. Chakraborty, E. Muljadi, and D. Maksimovic, "Rapid active power control of photovoltaic systems for grid frequency support," *IEEE J. Emerg. Sel. Topics Power Electron.*, vol. 5, no. 3, pp. 1154–1163, Sep. 2017.

[13] Y. Su, H. Li, Y. Cui, S. You, Y. Ma, J. Wang, and Y. Liu, "An adaptive PV frequency control strategy based on real-time inertia estimation," *IEEE Trans. Smart Grid*, vol. 12, no. 3, pp. 2355–2364, May 2021.

[14] Q. Peng, Z. Tang, Y. Yang, and F. Blaabjerg, "Event-triggering power reserve control for grid-connected PV systems," in *Proc. IEEE Appl. Power Electron. Conf. Expo. (APEC)*, New Orleans, LA, USA, Mar. 2020, pp. 417–423.

[15] S. Rivera, S. Kouro, B. Wu, J. I. Leon, J. Rodríguez, and L. G. Franquelo, "Cascaded H-bridge multilevel converter multistring topology for large scale photovoltaic systems," in *Proc. IEEE Int. Symp. Ind. Electron. (ISIE)*, Gdansk, Poland, Jun. 2011, pp. 1837–1844.

[16] R. You, X. Yuan, and X. Li, "A multi-rotor medium-voltage wind turbine system and its control strategy," *Renew. Energy*, vol. 186, pp. 366–377, Mar. 2022.

[17] H. D. Tafti, A. I. Maswood, G. Konstantinou, C. D. Townsend, P. Acuna, and J. Pou, "Flexible control of photovoltaic grid-connected cascaded H-bridge converters during unbalanced voltage sags," *IEEE Trans. Ind. Electron.*, vol. 65, no. 8, pp. 6229–6238, Aug. 2018.

[18] Q. Zhang, "Control of PV battery hybrid system using cascaded h bridge converter," in *Proc. IEEE 3rd Int. Future Energy Electron. Conf. ECCE Asia (IFEEC-ECCE Asia)*, Kaohsiung, Taiwan, Jun. 2017, pp. 2008–2012.

[19] X. Zhang, Y. Hu, W. Mao, T. Zhao, M. Wang, F. Liu, and R. Cao, "A grid-supporting strategy for cascaded H-Bridge PV converter using VSG algorithm with modular active power reserve," *IEEE Trans. Ind. Electron.*, vol. 68, no. 1, pp. 186–197, Jan. 2021.

[20] B. L. Xiao, L. Hang, C. Riley, L. M. Tolbert, and B. Ozpineci, "Modular cascaded H-bridge multilevel PV inverter with distributed MPPT for grid-connected applications," *IEEE Trans. Ind. Appl.*, vol. 51, no. 2, pp. 1722–1731, Mar. 2015.

[21] R. Sharma and A. Das, "A novel zero sequence voltage injection for extending active power balancing in grid tied solar PV powered cascaded H-bridge converter," in *Proc. IECON*, Lisbon, Portugal, Oct. 2019, pp. 4381–4386.

[22] C. Wang, K. Zhang, J. Xiong, Y. Xue, and W. Liu, "A coordinated compensation strategy for module mismatch of CHB-PV systems based on improved LS-PWM and reactive power injection," *IEEE Trans. Ind. Electron.*, vol. 66, no. 4, pp. 2825–2836, Apr. 2019.

[23] Y. Yu, G. Konstantinou, B. Hredzak, and V. G. Agelidis, "Power balance optimization of cascaded H-bridge multilevel converters for large-scale photovoltaic integration," *IEEE Trans. Power Electron.*, vol. 31, no. 2, pp. 1108–1120, Feb. 2016.

[24] A. I. Elsanabary, G. Konstantinou, S. Mekhilef, C. D. Townsend, M. Seyedmahmoudian, and A. Stojcevski, "Medium voltage large-scale grid-connected photovoltaic systems using cascaded H-bridge and modular multilevel converters: A review," *IEEE Access*, vol. 8, pp. 223686–223699, 2020.

[25] S. Y. Lee, Y. G. Jin, and Y. T. Yoon, "Determining the optimal reserve capacity in a microgrid with islanded operation," *IEEE Trans. Power Syst.*, vol. 31, no. 2, pp. 1369–1376, Mar. 2016.

XUEQING LI was born in Shandong, China, in 1997. He received the B.S. degree in electrical engineering and automation from the Qilu University of Technology, Jinan, China, in 2019. He is currently pursuing the M.S. degree with the College of Electrical Engineering, Qingdao University, Qingdao, China. His current research interests include the control of multilevel converters and photovoltaic generation technologies.

JIANYUN CHAI was born in Beijing, China, in 1961. He received the B.S. and Ph.D. degrees from the Department of Electrical Engineering, Tsinghua University, Beijing, in 1984 and 1989, respectively. Since 1989, he has been working at Tsinghua University, where he is currently a Professor of electric machinery and power electronics. His current research interests include wind energy generation, electric vehicle drives, integrated power and propulsion systems, and motion control.

MING LI was born in Hefei, China, in 1975. He received the B.S. and Ph.D. degrees in control theory and control engineering from Northeastern University, Shenyang, China, in 1997 and 2003, respectively. From 2003 to 2006, he was a Postdoctoral Fellow with the Electrical Automation Institute, Northeastern University. Since 2006, he has been working at the Ocean University of China, where he is currently a Professor of control engineering. His main research interests include marine renewable energy converter control, intelligent sensing, and autonomous control.

LIANGRAN LI was born in Weifang, China, in 1998. He received the B.S. degree in electrical engineering from Qingdao University, Qingdao, China, in 2020, where he is currently pursuing the M.S. degree with the College of Electrical Engineering. His current research interests include wind turbine control and renewable energy integration.

RUI YOU was born in Qingdao, China, in 1984. He received the B.S. degree in electrical engineering from Qingdao University, Qingdao, in 2006, the M.S. degree in electrical engineering from Shanghai Jiao Tong University, Shanghai, China, in 2009, and the Ph.D. degree in electrical engineering from Tsinghua University, Beijing, China, in 2015. He joined Qingdao University, in 2015, where he is currently working as an Associate Professor with the College of Electrical Engineering. His current research interests include wind turbine control, photovoltaic generation system control, and microgrid control.